Accepted Manuscript

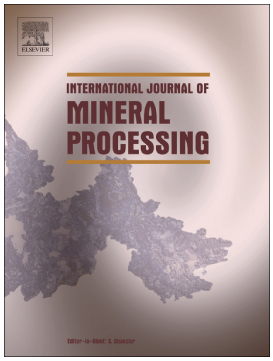

Quantifying of impact breakage of cylindrical rock particles on an impact load cell

Benjamin Bonfils

PII: S0301-7516(17)30027-3
DOI: doi: 10.1016/j.minpro.2017.02.005
Reference: MINPRO 3016

To appear in: *International Journal of Mineral Processing*

Received date: 31 August 2016
Revised date: 2 January 2017
Accepted date: 13 February 2017

Please cite this article as: Benjamin Bonfils , Quantifying of impact breakage of cylindrical rock particles on an impact load cell. The address for the corresponding author was captured as affiliation for all authors. Please check if appropriate. Minpro(2017), doi: 10.1016/j.minpro.2017.02.005

Quantifying of impact breakage of cylindrical rock particles on an impact load cell.

Benjamin Bonfils*

The University of Queensland, Sustainable Minerals Institute, Julius Kruttschnitt Mineral Research Centre
40 Isles Road, Indooroopilly, Brisbane, QLD 4068, AUSTRALIA
** T: +61 7 3365 5920 | F: +61 7 3365 5999 | E: b.bonfils@uq.edu.au*

Abstract. The detailed understanding of rock impact breakage represents a key challenge in the development of comminution models. Semi-empirical properties have been used to describe ore competencies, such as the JK breakage index t_{10} and Axb values, but are not able to estimate mechanical properties linked with particle fracture. The information derived from particle breakage testing on impact load cells devices, have the potential estimates such mechanical properties. However, the large intrinsic natural variability of rocks and ores composition and shape makes the results difficult to analyse and difficult to compare against each other for particles with similar properties. This study investigates the effect of rock shape on the variability of the impact breakage test conducted on impact load cells. The test methodology was modified to account for shape when testing regular shape samples such as drilled mini-cores, with objective of reducing the intrinsic variability caused by rock shape, using a controlled shaped sample. The promising results open new avenues for establishing relationships between rock composition, texture and mechanical properties.

Keywords: Comminution, fracture energy, rock shape, cylindrical rock, impact load cell

1. INTRODUCTION

The Impact Load Cell is a rock characterisation device based on the hybridisation of a drop weight tester and a Hopkinson bar. The technology was first developed at the Utah Comminution centre by Weichert (1986) and later detailed investigations with this device were carried out by King and Bourgeois (1993) and by Tavares and King (1998). A smaller portable version - the short impact load cell (SILC) - by Bourgeois and Banini (2002) was also designed with the aim of using it for in-situ testing. It has proven useful to measure rock particle fracture properties as detailed in published work by (King and Bourgeois, 1993; Tavares and King, 1998). The SILC measurements are used to derive material properties such as particle strength, particle stiffness and particle fracture energy. The fracture energy distribution of a sample is also used to investigate the intrinsic material variability of the tested sample.

A potential issue that can be encountered when comparing two rock samples tested on the SILC is that the measurement of individual particles captures the variability of the material as well as the shape variability, resulting in fracture energy distributions that can overlap or be hard to differentiate. There are several statistical testing methods to compare log-normally distributed fracture energies (Millin, 1994). The question then arises of the contribution of the shape variability of random irregular shaped particles in addition to the intrinsic material variability. Currently the SILC analysis assumes that the particles tested are spheres or a nearly spherical shape, which is an acceptable assumption when considering ore particles in a mineral processing circuit that have been conditioned through blasting, crushing or other size reduction processes. One possible solution to overcome this issue of shape variability is testing regular shaped particles. Of course the preparation of perfectly spherical rocks is practically impossible because of tedious and possible damaging processing of the rock particles. One relatively easy option is cutting the rocks to a desired shape. It is proposed in the present study that cylindrical rock cores are drilled into rock to produce a consistent cylindrical shape and thus the SILC results should reflect the variability due to the intrinsic properties of the rock rather than variability due to the irregular shape of the tested particles.

The main objective of this study is to show that the same mechanical properties can be derived when testing rock cylinders, eliminating variability due to the irregular shapes of crushed particles, potentially reducing the number of samples which need to be tested, and being able to test different mineral textures by drilling into selected ore phases that cannot be separated when preparing bulk samples of crushed particles. This methodology also opens new avenues for automation of impact load cell measurements with an easily handled particle that can be broken consistently and reducing sample preparation cost and time.

When conducting impact load cell measurements, the contact geometry between the striker, the particle and the bar has an influence on some of the measured properties and their calculation methodology. With any sample shape, the fracture force, or force at failure, of the specimen being impacted can be easily estimated from the force-time profile of the fracture event by direct reading of the peak force. The challenge resides in the calculations of the other fracture properties: fracture energy, stiffness and strength, which are influenced by the geometry of contact between the striker, the particle and the bar, as explained below. In previously published research the impact load cell measurement was applied to irregular shaped particles considered as spherical particles (King and Bourgeois, 1993; Tavares and King, 1998), as shown on Figure 1. Therefore the equations were easily derived from Hertzian contact theory (Goldsmith, 1960).

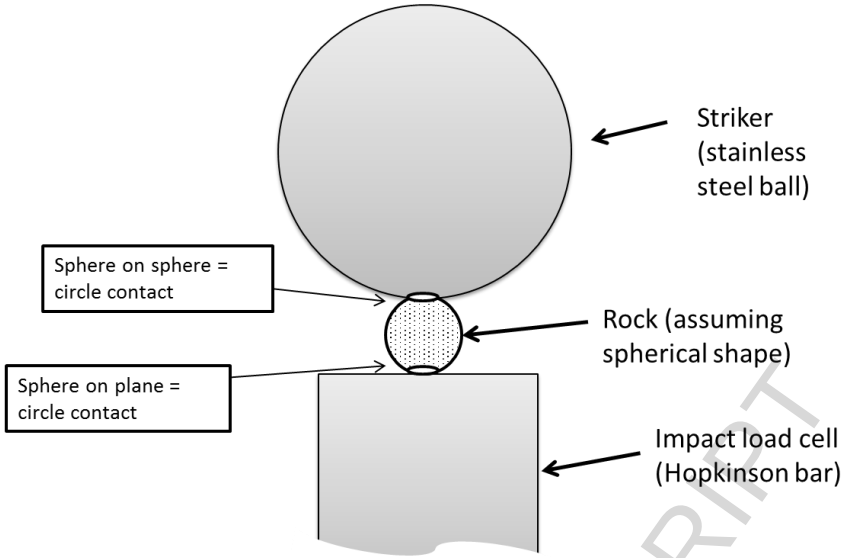

Figure 1 – Illustration of the bodies in contact in the case of a spherical particle during breakage in the impact load cell (cross sectional view).

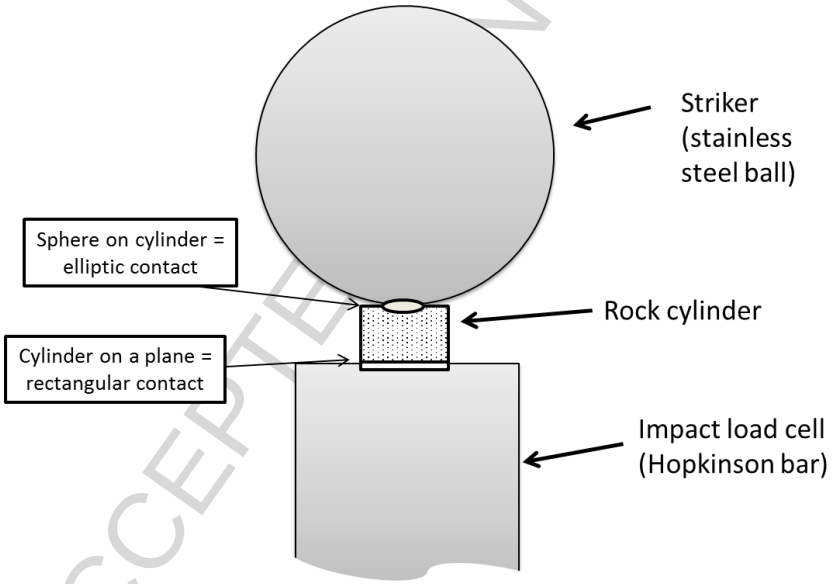

Figure 2 – Illustration of the bodies in contact in the case of a cylindrical particle on its side during breakage in the impact load cell (cross sectional view along cylinder axis).

In the case of rock cylinders the contact between striker, sample and impact load cell has a different geometry, as shown in Figure 2, and the equations for deriving material properties, such as fracture energy, need to be re-derived to account for the change of contact surface geometry. This paper presents the methodology developed to account for a cylindrical particle shape in the calculation of fracture energy in the impact load cell experiment. A validation test was carried out on a basalt sample to compare the fracture properties and material properties measured on crushed particles – considered spherical – and cylinders. The data shows good agreement and validates the proposed calculation methodology.

2. SAMPLE AND EQUIPMENT

2.1. Sample preparation

The sample used for demonstration of fracturing rock cylinders is a basalt from Bromelton Quarry in south-east Queensland (Australia). This basalt is a hard, brittle rock with homogeneous textural properties that makes it an ideal candidate when testing new breakage methodologies (Axb = 35). The sample was first crushed into a range of size fractions with irregular shaped particles. Larger particles from 10 mm to 25 mm in diameter were selected for drilling. A 8 mm diameter cylindrical diamond drill bit was used to drill into these particles and create the cylindrical shaped mini-cores. The cylinders were then cut using a diamond circular saw into identical lengths of 8 mm. The irregular shaped particles were sampled from the 5.6–6.7 mm size fraction of the crushed basalt for comparison with the mini cores. The size difference between the crushed particles equivalent diameter and the mini cores diameter is believed to have a small influence on the size-dependent properties.

2.2. Short Impact Load Cell device

The short impact load cell is based on the hybridisation of a drop weight tester and a Hopkinson bar. This impact load cell technology was developed by King and his co-workers Bourgeois and Tavares and details of the device have been published by these researchers (King and Bourgeois, 1993; Tavares and King, 1998, 2004). The short impact load cell used for this study was designed by Bourgeois and Banini (2002). The steel bar is equipped with strain gauges that are used to record the force applied on the particle during an impact by a striker. One of the hypothesis used to derive particle properties tested using SILC is that the particles are assumed to be spherical in shape. The equations shown by (Tavares and King, 1998) are only valid for particle shapes that are spherical (or nearly spherical). The calculation methodology developed for cylindrical shaped particles in this research is described below.

3. CALCULATION METHODOLOGY

The calculation methodology when breaking cylindrical rock particles lying on their side has been revised using the same methodology as in the previous literature but adapting it to a cylindrical rather than nearly spherical particle shape. The particle fracture energy corresponds to the elastic energy stored within a particle until the instant of fracture and corresponds to the area below the force deformation curve i.e.

$$E = \int_0^{\alpha_c} F d\alpha \tag{1}$$

where F is the applied load (or stress) and α is the deformation (or strain) applied on the particle. The details of the calculations of the deformation using the impact load cell will not be detailed in this study as they are similar to Eq. (6) of Tavares and King (1998). As mentioned before it was previously assumed that the deformation of a sphere on a flat surface impacted by a ball (Tavares and King, 1998) is described by

$$F = \frac{K_e d_p^{1/2}}{3} \alpha^{3/2} \tag{2}$$

where K_e is the local deformation coefficient of the Hertzian contact theory.

Unfortunately in the case of cylindrical rock particles this equation is not valid. In this case the actual deformation of the rock cylinder needs to be estimated before calculating the energy using Eq. (1). In order to calculate the deformation of the rock cylinder until the point of fracture, the deformation is a function of the force applied and the geometry of the bodies in contact. This can be predicted using Hertzian theory of contact for cylinders, sphere and planes.

For sake of clarity, the calculation methodology has been divided into two parts. The first part represents the contact of the impacting ball with the rock cylinder (sphere on cylinder). The second part represents the contact of the cylinder with the Hopkinson bar anvil (cylinder on flat surface). The total deformation of the rock cylinder can then be obtained by summing the deformation of each contact region.

3.1. Deformation of a cylinder in contact with a sphere.

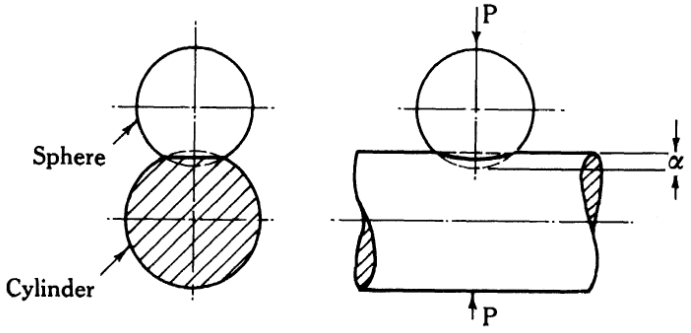

Figure 3 – Illustration of deformation of contact between a sphere and a cylinder, where *P* is the force applied, also named *F* in Eq (3), Eq. (4) and Eq (9). (From (Puttock, 1969))

Consider a sphere of diameter D_1 in contact with a cylinder of diameter D_2, with a force F exerted on the sphere, as shown in Figure 3. Puttock (1969) has defined the equation of deformation of the cylinder as function of the properties of the bodies in contact and of the force applied. In this case the shape of the contact area is an ellipse rather than the circular contact area seen in the case of two spheres in contact. The total elastic compression at the point of contact is

$$\alpha = \frac{2QF}{a} \times K \tag{3}$$

with

$$a^3 = \frac{2QF}{A} \times -\frac{1}{e}\frac{dE}{de} \tag{4}$$

where K and E are the complete elliptic integrals of first and second class respectively. They are calculated as shown in Eq. (5) and Eq. (6).

$$-\frac{1}{e}\frac{dE}{de} = \int_0^{\pi/2} \frac{sin^2\theta \, d\theta}{(1 - e^2 \, sin^2\theta)^{1/2}} \tag{5}$$

$$K = \int_0^{\pi/2} \frac{d\theta}{(1 - e^2 \, sin^2\theta)^{1/2}} \tag{6}$$

Q is a term defined by Puttock (1969) for bodies of different materials as

$$Q = \frac{3}{4\pi}\left(\frac{1}{k_1} + \frac{1}{k_2}\right) = \frac{3}{4 \, \pi \, K_e} \tag{7}$$

and K_e the local deformation coefficient of the Hertzian theory is

$$K_e = \frac{k_1 k_2}{k_1 + k_2} \tag{8}$$

where k_1 is the stiffness of the striker (steel in case of the SILC), and k_2 the stiffness of the rock cylinder. This equation is relevant to estimate the stiffness of the rock cylinder as explained later, since the stiffness of the stainless steel impactor and anvil are known values. Thus rearranging Eq (3),(4) and (7), and defining F as the force applied, the deformation of the contact between the sphere and the cylinder can be written as Eq. (9) where C is constant for a given cylinder and ball diameter. The elliptic integrals are a function of the diameter D_1 and D_2 and have been calculated in MATLAB for the dimensions of the impactor and the rock cylinders tested in this study.

$$\alpha = A^{1/3} . \frac{K}{\left(-\frac{1}{e}\frac{dE}{de}\right)^{1/3}} . \left(\frac{3F}{2\pi K_e}\right)^{2/3} = C \left(\frac{1}{D_1}\right)^{1/3} \left(\frac{3F}{2\pi K_e}\right)^{2/3} \tag{9}$$

3.2. Deformation of a cylinder in contact with a planar surface

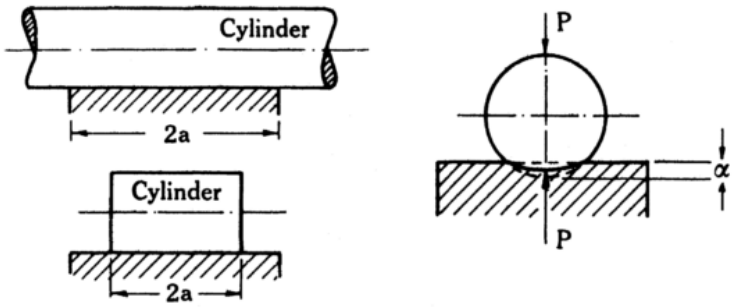

Figure 4 – Illustration of deformation of a cylinder in contact with a plane surface, where P is the force applied, also named F in Eq (10). (From Puttock (1969))

Consider a cylinder of length $L = 2a$ and dimeter D_2 in contact with a planar surface, with a force F exerted on the cylinder, as shown in Figure 4. As in the case of the sphere and cylinder described in the previous section, Puttock (1969) has defined the equation of deformation of the cylinder as a function of the properties of the bodies in contact and of the force applied. After rearranging we find that

$$\alpha = \frac{F}{L\pi K_e}\left(1 + \ln\left(\frac{2\pi K_e L^3}{FD}\right)\right) \tag{10}$$

with F being the force applied. The mechanical properties of bodies in contact (stiffness and local deformation coefficient K_e) conveniently remain the same in this case because, like the striker ball, the impact load cell is made of stainless steel. Now that the deformations associated with the contact of each side of the cylinders have been estimated, it is possible to calculate the cylinder fracture energy and the other fracture characteristics following the method described in section 5 of Tavares and King (1998).

3.3. Cylinder specific fracture energy

The total deformation in the vicinity of the contact is the sum of the deformation at the sphere-cylinder contact and the deformation at the cylinder-plane contact, that is Eq. (9) + Eq. (10). The fracture energy is calculated using Eq. (1) at point of fracture with α_c the deformation at the point of fracture and F_c the force at the point of fracture. For clarity, each part of the equation will be integrated separately, with the sphere-cylinder contact identified as $E_{s\text{-}c}$ and the cylinder-plane contact identified as $E_{c\text{-}p}$.

Firstly the energy for the sphere-cylinder side is calculated. Substituting Eq. (9) in Eq. (1) and integrating with a variable change from Δ_c to F_c, the energy can be related to the fracture force.

$$E_{s-c} = C\ \frac{2}{5D_1}\left(\frac{3}{2\pi K_e}\right)^{2/3} F_c^{\,5/3} \tag{11}$$

Then the energy for the cylinder-plane side is calculated. Differentiating Eq. (10):

$$d\delta = \left[\frac{1}{L\pi K_e}\left(1+\ln\left(\frac{2\pi K_e L^3}{FD}\right)\right)+\frac{F}{L\pi K_e}\left(-\frac{1}{F}\right)\right]dF = \frac{1}{L\pi K_e}\ln\left(\frac{2\pi K_e L^3}{FD}\right)dF \tag{12}$$

The energy of compression up to fracture is integrated between the initial contact and the instant of first fracture. At initial contact $\Delta = 0$ and $F = 0$, and at fracture $\alpha = \alpha_c$ and $F = F_c$.

Substituting Eq. (12) in Eq. (1) gives:

$$E_{c-p} = \frac{1}{L\pi K_e}\int_0^{Fc} F\ln\left(\frac{2\pi K_e L^3}{FD}\right)dF \tag{13}$$

Integration by parts was used to solve Eq. (13), and this gives the energy in Eq. (14).

$$E_{c-p} = \frac{F_c^{\,2}}{L\pi K_e}\left[\frac{1}{2}+ln\left(\frac{2\pi K_e L^3}{F_c\ D_1}\right)\right] \tag{14}$$

The calculations presented above allow calculation of the total energy used which is the sum of both integrals, Eq. (11) and Eq. (14). In the case of cylinders, equation Eq.(11) in Tavares and King (1998) becomes:

$$E = \frac{2}{5D_1}.C.\left(\frac{3}{2\pi K_e}\right)^{2/3} F_c^{\,5/3} + \frac{F_c^{\,2}}{L\pi K_e}\left[\frac{1}{2}+ln\left(\frac{2\pi K_e L^3}{F_c\ D_1}\right)\right] \tag{15}$$

The energy used during breakage E by the particle is measured by the Hopkinson bar according to Eq. (6) in Tavares and King (1998). Therefore K_e is the only unknown in Eq. (15), allowing calculation of the value of K_e using non-linear equation solving in Excel.

Then using Eq. (8) and knowing the stiffness of the stainless steel ball and rod, it possible to calculate the stiffness of the particle or cylinder. However, the energy absorbed by the particle (E') needs to be determined to account for the indentation of the platens in contact with the cylinder, as explained in Tavares and King (1998). The same methodology was used as in this study and the correction for actual energy absorbed as shown in Eq. (16) with k_p the particle (or cylinder) stiffness and $k_{b,r}$ the stiffness of the tools (which for stainless steel was assumed to be 230 GPa). The specific fracture energy E_m is simply obtained by dividing the fracture energy E' by the particle (or cylinder) mass.

$$E' = E\left(\frac{1}{\frac{k_p}{k_{b,r}}+1}\right) \tag{16}$$

4. RESULTS AND DISCUSSION

4.1. Comparative breakage experiment:

In order to validate the calculation methodology presented in this study, a comparative experiment was carried out on crushed particles and on cylindrical rock particles of the same material described earlier. Both types of particles were broken under single impact breakage conditions on the SILC device. The striker was a steel ball dropped onto the particle. The force-time profile was measured for crushed particles and for the rock cylinders. The impact conditions of each test are shown in the Table 1. An example of a force versus time breakage profile recorded by the impact load cell is shown in Figure 5 for the cylinders and in Figure 6 for the crushed particles.

Table 1 – Experimental conditions of the single impact breakage tests on the SILC.

	Crushed particles	Rock cylinders
Size fraction (mm)	5.6-6.7	8.27 (diameter) (standard deviation = 0.304)
Number of particles	28	22
Average mass (g)	0.34	1.23 (standard deviation = 0.055)
Average height (mm)	5.1	8.27
Ball diameter (mm)	50.8	60
Ball mass (g)	550.35	880.55
Drop height (mm)	65	70.5

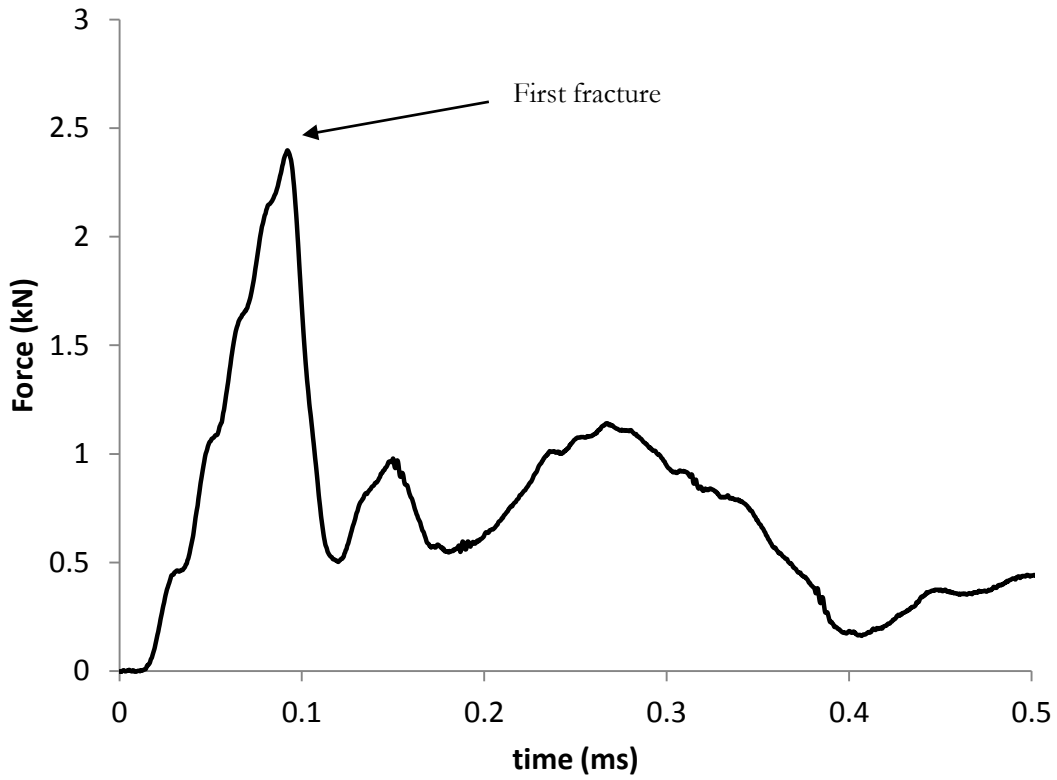

Figure 5 – Example of force versus time profile recorded using SILC during the impact event of a rock cylinder. The force to first fracture peak is shown.

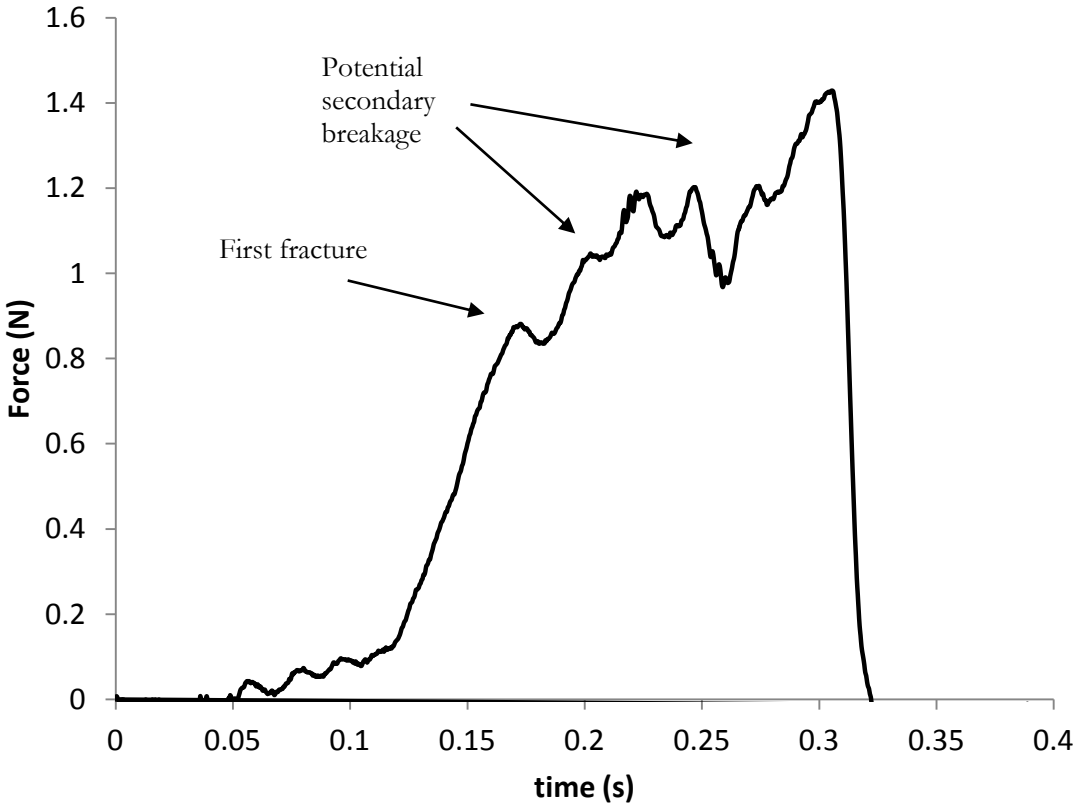

Figure 6 – Example of force versus time profile recorded with SILC during impact event of an irregular shaped particle. The first fracture event is shown and potential secondary breakage due to capture of the broken fragments.

It was observed that all of the force-time profiles recorded when breaking the cylinder shaped rock were similar to the one shown in Figure 5. It is quite intuitive to select the peak corresponding to the fracture force showed by a steep drop in the force corresponding to the fracture. The sphere impact resulted in splitting of the cylinder along the core diameter, as illustrated in Figure 5. Because of the systematic shape of the force signal, an automated peak detection could be implemented instead of having the user select the peak force for the irregular shape material. When analyzing the curves recorded for the crushed particles as shown in Figure 6, the peak force was less distinct, which could be caused by secondary breakage of the fragments produced after the first fracture, due to the momentum of the striker that keeps falling towards the anvil and impacts the irregular shaped fragments.

4.2. Analysis of the particle fracture energy distribution and stiffness:

The fracture energy and particle stiffness were calculated using the calculation methodology presented in the previous section for the rock cylinders and using the methodology explained in (Tavares and King, 1998) for the crushed particles which are considered as spherical. The specific fracture energy was calculated for all broken particles and is shown in Figure 7.

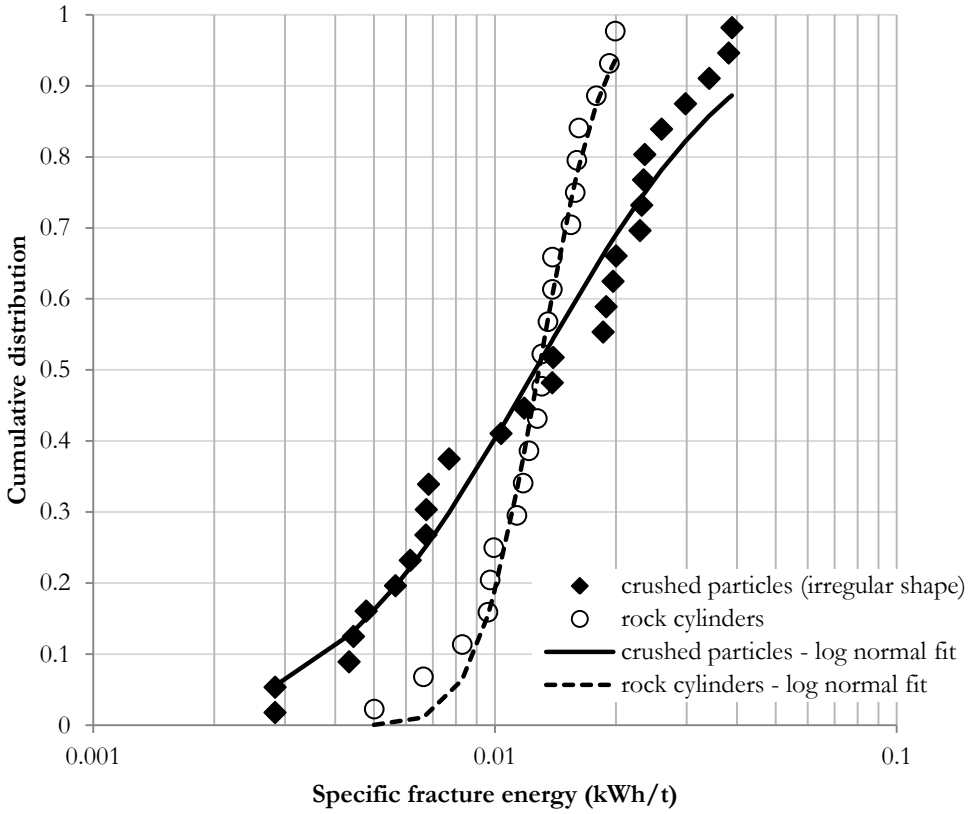

Figure 7 – Cumulative distribution of the specific fracture energies calculated for the crushed particles and for the rock cylinders.

It was observed that the fracture energies measured for crushed particles and for the rock cylinders have closely matching median values, but different standard deviations. Indeed, it is apparent that the distribution for the rock cylinders is sharper than for the irregular shaped particles. The fracture energy is also size dependent (King and Bourgeois, 1993; Tavares and King, 1998), but the sizes of the tested particles (5.6-6.7mm) and cylinders (8 mm) were selected to avoid any measurable effect due to size dependency thus similar fracture energies would be expected.

The cumulative distribution was modelled using the lognormal distribution to describe the specific fracture energy (or fracture probability) using Eq. (17) (King and Bourgeois, 1993; Tavares and King, 1998). A least squares minimization was used to estimate the distribution parameters $E_{m,50}$ and ${\sigma_E}^2$, which are the median and the geometric variance of the distribution respectively.

$$P(E_m) = \frac{1}{2}\left[1 + \text{erf}\left(\frac{\ln E_m - \ln E_{m,50}}{\sqrt{2{\sigma_E}^2}}\right)\right] \quad (17)$$

The log normal distribution parameters were used to compare the distributions obtained with irregular crushed particles and with the rock cylinders, as shown in Table 2. The parameters confirm the observations made on Figure 7, that the median specific fracture energy is similar for the irregular particles and cylinders, and the variance of the distribution was significantly reduced for the cylinders (by a factor 10). In addition, the accuracy of testing device, which is linked to the resolution of the strain gauge and digitalisation equipment is significantly lower than the variability observed for each sample. The resolution of the equipment is ± 5 N, which is about 0.2% of the measured fracture force recorded.

Table 2 – Lognormal distribution parameters obtained for the irregular shaped particles and for the rock cylinders.

	Cylinders	Crushed particles
Fitted $E_{m,50}$ (kWh/t)	0.01286	0.01257
Fitted σ_E^2 ((kWh/t)²)	0.0829	0.8715

The results, and accuracy of the measurements, lead to the conclusion that the variability observed for the irregular shaped particles is caused by both the shape variability and the intrinsic material variability. As expected, the controlled cylindrical shape has helped to reduce the variability of the results without compromising the measure of the average material properties which is the specific fracture energy. Similar observations were obtained when comparing the stiffness of the particles calculated using Eq. (8), as shown in Figure 8.

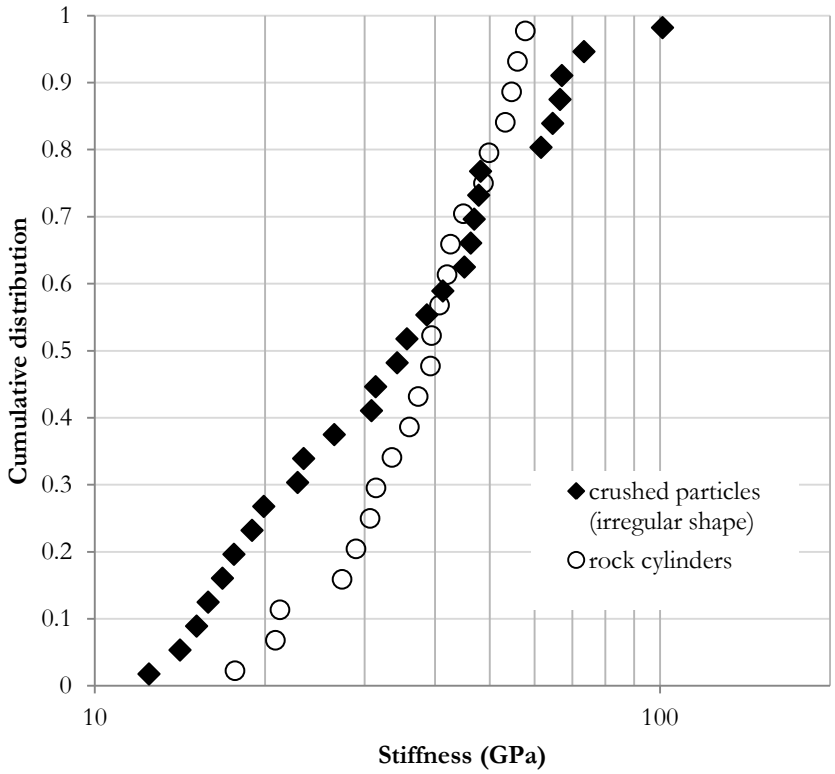

Figure 8 – Cumulative distribution of the material stiffness calculated for the crushed particles and for the rock cylinders.

The variability of the measurements influences the number of particles to be tested and the confidence in the values measured. This study shows the opportunity to measure particle properties with a reduced number of samples by using a controlled particle shape. It should be emphasised that the material tested in this experiment is a relatively homogeneous rock that is expected to give very consistent results. In the case of a real ore, the lithology of the ore will influence the variability of the measured fracture energies and the experiment cannot differentiate between mineral textures when a representative sample of crushed material is being tested. However, the method of preparation of the cylinders potentially allows users to select particular zones within a natural ore by drilling into specific mineral phases and testing them separately. This method opens new avenues for modelling the breakage of heterogeneous mineral ores by treating them as composites of mineral textures with different competencies.

4.3. Estimation of the Tensile Strength

The testing configuration of the cylinder compressed by two plates is similar to the standard Brazilian test where the stress applied is normal to the splitting diameter – cylinder on its side (ISRM, 2006). As opposed to the Brazilian test, the impact in the SILC test is dynamic – with the ball falling – and the curved surface of the ball is in contact with the top of the cylinder whereas a planar or concave surface is used in the Brazilian test. As mentioned before, the fragmentation mechanism observed in the tests performed in this study on the cylinder is equivalent to the splitting mechanism in the Brazilian test. Therefore, it was proposed that the same equation can be used in the test to estimate the tensile strength of the material, as shown in Eq. (18) with F_c the fracture force, D the cylinder diameter and L the cylinder length (or thickness in the Brazilian test) (ISRM, 2006).

$$\sigma_T = \frac{2\,F_c}{\pi\,D\,L} \tag{18}$$

The tensile strength was calculated for the 22 cylinders tested and the average was: σ_T = 9.31 MPa with a standard deviation of 2.35. The Brazilian tensile strength of the sample used in this study was not measured using the standard methodology (ISRM, 2006), but this value is in agreement with values quoted in the literature for a basaltic rock. Çanakcı et al. (2008) found 8.3 MPa average with SD = 2.1. Similar values between 8 and 12 MPa were found by Kahraman et al. (2012) and by Schultz (1993) for other basalt samples.

In addition to the specific fracture energy and stiffness, the proposed testing methodology presented here can also be used to estimate the tensile strength properties of the material tested, with a simple and cost effective sample preparation and testing compared to the standard methodology.

4.4. Discussion about the effect of pre-selection in sample preparation

It was observed during sample preparation that not all of the drilled particles produced a cylinder for testing. Some particles failed during drilling due to the rotational force applied by the drill. The mini-cores that were measured by the SILC test were those that survived the drilling process and this creates a bias in the results. If a crack or fault existed in the rock structure before drilling, the core extracted during drilling might be fragmented into several sections that may not be adequate for testing, for example the core may be too short. This selection of the intact cores can impact the final distribution of measured fracture energies and fracture properties. The author believes that this will not have a significant impact considering the homogeneous texture of the tested basalt. However it could have a more significant impact when testing heterogeneous rock textures where particles separate into components of various competence and where it may be impossible in practice to obtain an intact cylinder of brittle material. Further investigations will be required to study this effect when investigating real ores.

5. CONCLUSIONS

A new SILC testing and calculation methodology has been developed which accounts for particle shape by testing cylindrical shape particles instead of nearly spherical shaped particles. A validation test with basalt rock showed that the variability of the material properties measured was significantly reduced by controlling the shape of the particles. The variance of the distribution of fracture energies for the cylindrical rock was reduced by 10 times compared to the irregular shaped particles. Both the median specific fracture energy and the material stiffness were equivalent for the irregular shape particles and cylinders. It was also possible to derive the equivalent Brazilian tensile strength for the same measurement using the dimensions of the cylinders and the fracture force.

The proposed methodology and reduced variability in the distribution of fracture energies can be used to differentiate materials with different characteristics such as mineralogical composition within an ore body, where the variability measured using irregular shaped material made them statistically impossible to differentiate. This methodology has been successfully applied by Yildirim et al. (2016, thesis in print) and will be published in a separate paper.

Using rock cylinders as the test material also opens new avenues for automated SILC impact testing with the regular particle geometry allowing easy preparation and handling of the particles, as well as automated force signal post-processing. There may also be opportunities for selective drilling and independent testing of mineralogical phases within complex and variable ore bodies to investigate the effect of texture and ore composition on the material properties such as the mechanical texture concept introduced by Bourgeois et al. (2015).

6. ACKNOWLEDGMENTS

The author would like to thank Baris Yildirim, Ph.D. Scholar at JKMRC for his contribution and for helping with sample preparation and testing. The research presented in this paper was supported by the University of Queensland Strategic Funding.

7. REFERENCES

Bourgeois, F.S., Banini, G.A., 2002. A portable load cell for in-situ ore impact breakage testing. International Journal of Mineral Processing 65, 31-54.
Bourgeois, F.S., Lippiatt, N.R., Powell, M.S., 2015. Introducing the concept of mechanical texture in comminution: The case of concrete recycling. International Journal of Mineral Processing 136, 7-14.
Çanakcı, H., Baykasoğlu, A., Güllü, H., 2008. Prediction of compressive and tensile strength of Gaziantep basalts via neural networks and gene expression programming. Neural Computing and Applications 18, 1031-1041.
Goldsmith, W., 1960. Impact : the theory and physical behaviour of colliding solids. London : Arnold, London.
ISRM, 2006. The Complete ISRM Suggested Methods for Rock Characterization, Testing and Monitoring: 1974-2006.
Kahraman, S., Fener, M., Kozman, E., 2012. Predicting the compressive and tensile strength of rocks from indentation hardness index. Journal of the Southern African Institute of Mining and Metallurgy 112, 331-339.
King, R.P., Bourgeois, F., 1993. Measurement of Fracture Energy during Single-Particle Fracture. Minerals Engineering 6, 353-367.
Millin, L.K., R.P., 1994. Testing the equality of two independent distribution of data on the Ultrafast Load Cell. University of Utah, U.S.A, The Utah Comminution Centre, p. 36.
Puttock, M.J.T., E.G., 1969. Elastic Compression of Spheres and Cylinders at Point and Line Contact. CSIRO, National Standards Laboratory Technical Paper No. 25.
Schultz, R.A., 1993. Brittle strength of basaltic rock masses with applications to Venus. Journal of Geophysical Research: Planets 98, 10883-10895.
Tavares, L.M., King, R.P., 1998. Single-particle fracture under impact loading. International Journal of Mineral Processing 54, 1-28.
Tavares, L.M., King, R.P., 2004. Measurement of the load–deformation response from impact-breakage of particles. International Journal of Mineral Processing 74, S267-S277.
Weichert, R.H., J.A, 1986. An ultrafast load cell device for measuring particle breakage, Prepr. 1st World Congr. Particle Technology, Nürnberg II, pp.3